https://doi.org/10.5194/egusphere-2025-5977
Preprint. Discussion started: 6 January 2026

Near Real-Time & Benchtop XRF Intercomparison for PM Elemental Analysis on Quartz and Teflon Filters: A Case Study Across Three European Cities

Stefanos Papagiannis[1,2], Manousos I. Manousakas[1], Dimitrios F. Anagnostopoulos[2], Michael Pikridas[3], Rima Baalbaki[3], Jean Sciare[3], Niall O'Sullivan[4], Stig Hellebust[4], John Wenger[4], Kirsten N. Fossum[5], Jurgita Ovadnevaite[5], Anja Tremper[6], David Green[6], Konstantinos Eleftheriadis[1], Evangelia Diapouli[1]

[1]ENvironmental Radioactivity & Aerosol Technology for atmospheric & Climate ImpacT Lab (ENRACT), Institute of Nuclear and Radiological Science & Technology, Energy & Safety, NCSR Demokritos, Athens, 15310, Greece
[2] Department of Materials Science & Engineering, University of Ioannina, Ioannina, 45110, Greece
[3]Climate and Atmosphere Research Center, The Cyprus Institute, Nicosia, 2121, Cyprus
[4]School of Chemistry and Sustainability Institute, University College Cork, Cork, T12 K8AF, Ireland
[5]School of Natural Sciences, Ryan Institute's Centre for Climate & Air Pollution Studies, University of Galway, Galway, H91 TK33, Ireland
[6]MRC Centre for Environment and Health, Environmental Research Group, Imperial College London, London, W2 1PG, United Kingdom

Correspondence to: Stefanos Papagiannis (s.papagiannis@ipta.demokritos.gr), Evangelia Diapouli (ldiapouli@ipta.demokritos.gr)

Abstract. This study presents an extensive intercomparison between a benchtop X-ray fluorescence (XRF) system and near real-time XRF monitors (Xact 625 and 625i) for measuring elemental concentrations in ambient aerosols. The measurements were conducted across three locations: Athens (Greece, March 2024), Nicosia (Cyprus, March–January 2023), and Dublin (Ireland, December 2022–February 2023). The focus was on evaluating the chemical composition of particulate matter (PM) and the impact of filter substrate choice on measurement consistency. The study specifically examines the elements Si, S, Cl, K, Ca, V, Ti, Mn, Fe, Cu, Ni, Zn, Sr, and Pb. The results highlight that filter type plays a crucial role in ensuring accurate measurements when utilizing the benchtop XRF system. At the Athens site, where PTFE filters were used, the agreement between the Xact 625i and the benchtop XRF system was stronger, with slopes generally closer to unity for most elements. In contrast, quartz fiber filters at the Dublin and Nicosia sites led to systematic deviations, especially for light elements such as S, Cl, and K, even after applying correction factors. For heavier elements like Fe, Mn, and Cu, the filter effect was less pronounced, though some variation across sites remained. Zn consistently showed good agreement, while Pb exhibited weaker correlation, possibly due to differences in the calibration curves of the two systems. Overall, this study not only evaluates instrument performance across multiple environments but also provides practical guidance for mitigating filter-related artifacts to enhance consistency in elemental aerosol measurements.

https://doi.org/10.5194/egusphere-2025-5977
Preprint. Discussion started: 6 January 2026

1 Introduction

Particulate matter (PM) is a well-known major atmospheric pollutant, originating from both natural and anthropogenic sources, with significant impacts on health (Ostro et al., 2015; Samoli et al., 2013) and climate (Chen et al., 2021). Composed of a complex blend of chemical components, such as carbonaceous, ionic, and elemental species, the PM's composition varies widely depending on sources and environmental conditions, which contributes to its diverse chemical and physical characteristics.

The elemental analysis of atmospheric aerosols can offer information of critical value for health and source apportionment studies, which are vital for understanding pollution sources (Manousakas et al., 2021; Hopke et al., 2020), assessing population exposure risks (Megido et al., 2017; Caggiano et al., 2019), and implementing effective air quality management strategies. Exposure to certain elements, including As, Ni, Cr, Cd, and Pb, has been associated with an elevated cancer risk via inhalation (Aldekheel et al., 2023). These trace elements are also implicated in disrupting respiratory health by impairing mucociliary clearance, weakening barrier functions, inducing airway inflammation, promoting oxidative stress, and triggering cell apoptosis (Skalny et al., 2020).

Although elemental species do not substantially contribute to the overall mass of PM, they are crucial for accurately identifying pollution sources. The chemical signatures of the processes are mirrored in the emitted aerosol particles, enabling the use of specific elements to trace and allocate the sources of ambient aerosols effectively (Viana et al., 2008; Amato et al., 2016; Diapouli et al., 2017). For example, crustal elements like Al, Si, Ca and Fe serve as indicators of mineral dust (Viana et al., 2008; Jain et al., 2020); Cu and Zn are markers of brake and tire wear (Rhodes et al. 2012; Huang et al. 2018; Thorpe and Harrison 2008); Br and Cl are indicators of coal combustion (Papagiannis et al., 2024); and V and Ni may point to heavy oil combustion (Jang et al., 2007; Healy et al., 2009).

Clearly, the accurate assessment of the elemental composition of ambient aerosols is of vital importance. PM emissions and atmospheric dynamics, influenced by factors like wind direction and precipitation, can fluctuate within hours, affecting aerosol concentration and composition. Sampling on an hourly timescale (or at even higher time resolution) allows for a more detailed understanding of emission, transport, and deposition processes, enabling the capture of rapid source impacts. The recent advancements in high-time-resolution elemental analysis, especially by energy dispersive X-ray fluorescence (ED-XRF) spectrometers such as the Xact 625 and Xact 625i (SailBri Cooper, Inc.), have significantly enhanced the ability to identify and trace pollution sources with greater precision (Manousakas et al., 2022; Rai et al., 2020). In addition, those near real-time XRF spectrometers (NRT-XRF) also allow automated sampling of both PM_{10} and $PM_{2.5}$ which greatly enhances the information regarding aerosol composition (Furger et al., 2020).

A focused comparison of benchtop ED-XRF and NRT-XRF spectrometers, specifically regarding the measured elemental concentrations, is essential to determine their effectiveness in elemental monitoring of ambient aerosols. While past studies have evaluated the performance of NRT-XRF instruments, specifically the Xact 625 and 625i (Windell et al., 2025), these comparisons primarily involved ICP-MS (Furger et al., 2017; Tremper et al., 2018; Bhowmik et al., 2022) and, in only

https://doi.org/10.5194/egusphere-2025-5977
Preprint. Discussion started: 6 January 2026

one case, the comparison of a benchtop ED-XRF spectrometer with an earlier Xact 625i model (Cadeo et al., 2025). This limited research underscores the need for a direct, updated comparison between current NRT and benchtop ED-XRF instruments to validate their performance in real-world conditions and to assess whether NRT-XRF could potentially replace traditional methodologies.

In addition to the need for direct instrument comparison, the choice of filter substrate significantly affects quantitative PM analysis in ED-XRF spectrometry (Unga et al., 2025). Within many air quality monitoring networks, high-volume samplers routinely employ quartz fiber filters because of their compatibility with subsequent analyses of organic and ionic species. When extending these existing measurements to include elemental or metal characterization, it is often more practical to use the already collected quartz filters rather than perform additional co-located sampling on Teflon filters. However, this approach requires careful consideration of substrate-related effects. While many studies have examined Teflon and quartz fiber filter differences for organic and ionic species (Vecchi et al., 2009; Khuzestani et al., 2017; Aikawa and Hiraki 2010), there is limited literature regarding elemental characterization (Chiari et al., 2018; Yatkin et al., 2012). Chiari et al. (2018) emphasized the challenges when working with quartz fiber filters, which can introduce self-absorption and matrix effects due to their thickness, potentially leading to very high inaccuracies in concentration measurements, especially for lighter elements. Corrective methods are therefore essential when using quartz fiber filters to obtain accurate elemental concentrations.

For the reasons above, this study focuses on a detailed comparison between a benchtop ED-XRF and near real-time (NRT) XRF spectrometers (specifically the Xact 625 and 625i models) for measuring elemental concentrations in ambient aerosols, alongside an evaluation of filter substrate performance. Measurement campaigns were conducted in Athens, Greece (March 2024), Nicosia, Cyprus (March 2022–January 2023), and Dublin, Ireland (December 2022–February 2023), including quartz fiber and Teflon substrates for the comparison. Additionally, a dedicated filter substrate campaign was performed in January 2024. The results will compare the two instrument types across different environments and timeframes, providing insights into their consistency and applicability. Furthermore, the filter substrate comparison will assess the impact of Teflon and quartz fiber filters on elemental quantification and offer practical recommendations for corrective procedures in aerosol studies.

2 Experimental

2.1 Sampling and Study area

Athens N.C.S.R. “Demokritos” station (ATH-DEM):

Measurements in Athens, specifically in Agia Paraskevi, were conducted at the urban background monitoring station located on the N.C.S.R. “Demokritos” campus (37°59'42.0"N, 23°48'57.6"E; 270 m above sea level) (Figure 1). This station is approximately 7 km northeast of central Athens and is situated at the base of Mount Hymettus. The station is part of the PANACEA National Infrastructure for Greece and provides representative data to the ACTRIS European infrastructure on

https://doi.org/10.5194/egusphere-2025-5977
Preprint. Discussion started: 6 January 2026

urban background air quality due to its location, which is largely unaffected by direct emissions from urban PM sources (Zografou et al., 2022, Eleftheriadis et al., 2021).

A 24-hour sampling campaign took place from March 5 to March 25, 2024, resulting in 21 $PM_{2.5}$ samples. These samples were collected using Teflon filters (PTFE Pall R2PJ047 with PMP support ring, 47 mm diameter, 2 µm pore size) on a low-volume sampler (Sequential 47/50-CD, Sven Leckel GmbH, Berlin, Germany) operating at a flow rate of 2.3 m³/h. In addition, an earlier campaign was conducted from January 13 to January 31, 2024, to investigate potential differences in elemental composition when using different filter substrates. This included 21 PM_{10} samples collected on Teflon filters (WHATMAN – PTFE, polypropylene-backed, pore size 1.0 µm, diameter 47 mm) and 21 PM_{10} samples collected on quartz fiber filters (PALLFLEX Tissue Quartz).

Cyprus Atmospheric Observatory (CAO-NIC):

Sampling was conducted at the Cyprus Atmospheric Observatory (CAO-NIC) urban background station of the Cyprus Institute premises in Nicosia (Athalassa Campus; 35°08'27.6"N 33°22'51.6"E; 174 m above seal level) (Figure 1). The site is located in a low-density residential area and is approximately 800 meters from the nearest major road and far from other significant anthropogenic sources. The Athalassa Forest Park lies to the southeast of the institute, further contributing to the minimal local pollution influences. Source apportionment studies (Bimenyimana et al., 2025; Bimenyimana et al., 2023; Christodoulou et al., 2023) show that PM at the site originates from a complex blend of local and regional sources. Regional air masses vary seasonally, bringing sulfate-rich air from Turkey and Eastern Europe in summer and dust mixed with anthropogenic pollutants from the Middle East and North Africa during other seasons. Local sources include biomass burning, traffic, power generation, and shipping activities.

$PM_{2.5}$ particles were collected on 47-mm diameter quartz filters (Tissuquartz 2500QUAT-UP, Pall) at 10 m above ground level (AGL)using a Leckel SEQ47/50 sampler operating at a flow rate of 2.3 m³/h and utilizing. After collection, the filters were placed in petri dishes and stored at -18 °C until further analysis. To ensure the proper functioning of the sampler, regular flow checks were performed throughout the campaign. A total of 256 filters were utilized over the course of the measurement period, from March 18, 2022, to January 17, 2023. Most samples were taken over 24-hour intervals, from 00:00 to 00:00 UTC. However, between December 16, 2022, to January 17, 2023, the sampling frequency was increased to every 8 hours corresponding to three collection periods: 02:00 – 10:00, 10:00 – 18:00, and 18:00 – 02:00.

Dublin Port Station (DUB-P):

Measurements were conducted in Dublin Port from 16 December 2022 to 7 February 2023 as part of the research project Source Apportionment of Air Pollution in the Dublin Port Area (PortAIR) (Fossum et al., 2025). Aerosol physicochemical properties and gaseous pollutants were measured using a suite of instrumentation housed in two containers. The monitoring site (53°20'54.4"N 6°11'40.8"W) (Figure 1) was selected to be downwind of most port activity and close to the ferries, which are a major daily source of shipping emissions (Fossum et al., 2024). A total of 54 $PM_{2.5}$ samples were collected onto quartz

https://doi.org/10.5194/egusphere-2025-5977
Preprint. Discussion started: 6 January 2026

fiber filters (Pallflex, 150 mm diameter), pre-baked for 3 hours at 850°C, using a high-volume sampler (model DHA 80, Digitel) operating at a flow rate of 500 L min^{-1}. Following collection, the filters were individually packed and stored in a freezer at −18°C. until analysis.

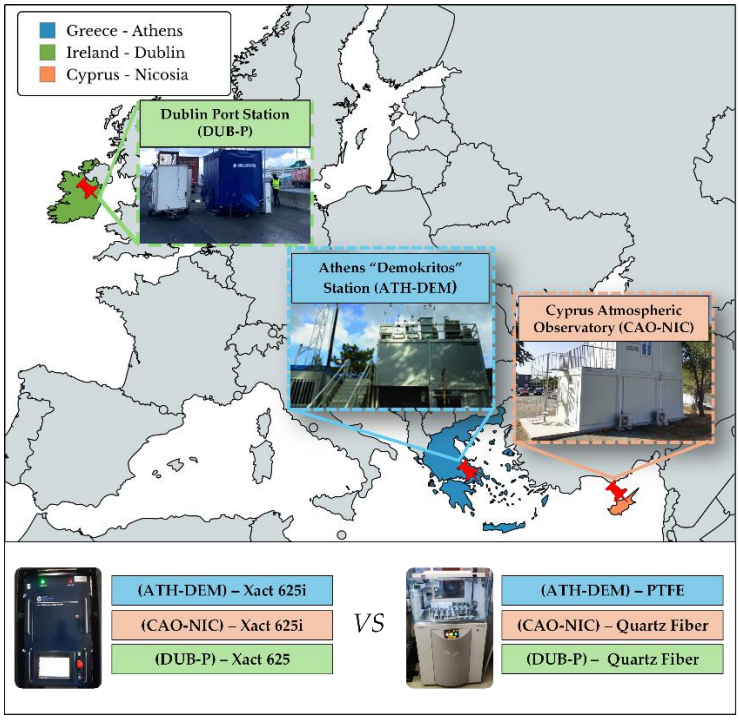

Figure 1: Locations of the measurement campaigns conducted in this study.

2.2 Instruments

2.2.1 Benchtop ED-XRF spectrometer

$PM_{2.5}$ samples were analysed for major and trace elements using a high-resolution energy-dispersive X-ray fluorescence (ED-XRF) spectrometer with advanced 3-D optics, the Epsilon 5 (PANalytical). The spectrometer features a side-window, low-power X-ray tube equipped with a tungsten/scandium (W/Sc) anode. The characteristic X-ray radiation emitted by the samples is detected by a germanium (Ge) detector, offering an energy resolution of approximately 150 eV full-width at half-maximum (FWHM) at the Mn-Kα line (5.89 keV). To enhance measurement precision, the system employs six secondary targets (CaF_2, Ge, Mo, KBr, Al_2O_3, and LaB_6) that polarize the X-ray beam, allowing for six optimized measurement conditions tailored to the analysis of aerosol samples.

Calibration of the ED-XRF spectrometer was performed using a range of reference standards, including infinitely thin, single-element, compound, and multi-element materials. Specifically, 27 Micromatter thin-film standards deposited on 6.3 µm Mylar substrates were utilized, encompassing materials such as NaCl, MgF_2, GaP, SiO, KCl, CaF_2, V, Fe, Cr, Co, CuS_x, Al, Ni, CsBr, RbI, SrF_2, Ge, Se, Ag, Sn, Sb, Pt, AgHg, CdSe, Pb, Au, BaF_2, and Ce. Additionally, 22 multi-element

https://doi.org/10.5194/egusphere-2025-5977
Preprint. Discussion started: 6 January 2026

standards were used, including one SRM 2783 standard and 21 UCDAVIS standards on polycarbonate and Teflon substrates. The reported uncertainty for Micromatter standards is 5%, while for multi-element standards, it is 10%. Each sample underwent a 60-minute analysis. The detection limits are calculated using the equation (Manousakas et al., 2018):

$$LoD = \frac{3\sqrt{Bkg}}{I\,t}\ \frac{1}{S} \quad (1)$$

here, LoD represents the detection limit in μg/cm², Bkg denotes the background counts of a field blank filter over a FWHM region centered at the element's principal peak centroid, I is the tube current in mA, t is the measurement time in seconds (s), and S refers to the sensitivity in $(\frac{counts}{s\,mA})/(\frac{\mu g}{cm^2})$. Figure 2a presents the detection limits for the measured elements on PTFE and quartz fiber blank filters in ng m-3. To express the concentrations and detection limits in volumetric units (ng/m³), values in μg/cm² were first multiplied by the effective area of the filter (cm²) and then divided by the total sampled air volume (m³). This conversion accounts for the sampled air mass per unit volume and allows for direct comparison with ambient air quality standards.

The Quality Assurance/Quality Control (QA/QC) protocol for analysis includes a series of procedures to ensure high data quality and reliable instrument performance. The procedures involve: a) Weekly calibration of the Ge detector – The XRF software automatically fine-tunes the energy channels to maintain optimal detector performance; b) Regular performance evaluation using SRM 2783 – Weekly analyses of the multi-element reference material are conducted to verify analytical accuracy and precision for each analyte; c) Daily monitoring with PTFE blanks – Selected PTFE blank samples are systematically analysed to assess long-term reproducibility and ensure consistency across measurements. Limits of detection for PTFE and Quartz fiber filters are presented in Table S1 in ng m^{-3}.

2.2.2 Near real-time (NRT) XRF spectrometers

The study utilized near real-time XRF spectrometers at three locations: Athens, Greece (ATH-DEM station, Xact 625i, Cooper Environmental Services (CES), Beaverton, OR, 129 USA), Dublin, Ireland (DUB-P station, Xact 625 Cooper Environmental Services (CES), Beaverton, OR, 129 USA), and Nicosia, Cyprus (CAO-NIC station, Xact 625i, Cooper Environmental Services (CES), Beaverton, OR, 129 USA).

The Xact systems (625 and 625i) used in this study operate at a flow rate of 1 m³/h through a $PM_{2.5}$ cyclone, collecting particles on Teflon filter tape and analysing them hourly. During each cycle, the collected sample is irradiated using a 50 kV, 50 W Rh-anode X-ray tube, and the resulting fluorescence is recorded by a silicon drift detector. Spectra are processed using the manufacturer's software to quantify elemental concentrations. The instruments run continuously, with simultaneous sampling and analysis, and routine QA checks (flow, calibration stability) performed daily and at campaign start/end. The Xact 625 deployed in Dublin (16 December 2022–7 February 2023) reported up to 24 elements (Si–U) and used a heated inlet (45 °C) when relative humidity exceeded 45%. The Xact 625i instruments in Athens (5–25 March 2024) and Nicosia (18 March 2022–17 January 2023) measured up to 35 elements (Al–Pb) under otherwise similar operating conditions.

https://doi.org/10.5194/egusphere-2025-5977
Preprint. Discussion started: 6 January 2026

The limits of detection for the Xact 625i and 625 are determined for each element using its sensitivity and the background counts from a blank, unused section of the tape. The reported values correspond to 1σ interference-free detection limits. For this study, a 60-minute time resolution was used. The limits of detection for Xact 625 and 625i are calculated using the equation (Rai, 2020):

$$LoD_{\sigma_0} = \frac{\sigma_0}{V} = \frac{\sqrt{Bkg\ t\ I}}{S\ t\ I}\ \frac{1}{V} \quad (2)$$

where, σ_0 represents the 68% confidence level detection limit, Bkg is the background count rate in $counts/(s\ \mu A)$, t is the live time in seconds (s), I is the current in μA, S is the sensitivity in $(\frac{counts}{s\ mA})/(\frac{\mu g}{cm^2})$ and V is the sample volume in m^3. Figure 2b presents the LoDs of the Xact 625 and Xact 625i spectrometers in ng/m³.

Quality assurance procedures for the Xact 625 and Xact 625i included daily energy calibration, response-stability checks for Cd, Cr, and Pb, and independent flow-rate verifications. The Xact 625 uses Palladium (Pd) as its internal calibration standard, whereas the Xact 625i uses Niobium (Nb). Tape blanks were collected before and after filter-tape changes to ensure accuracy. Calibration with thin-film standards was performed when necessary to maintain measurement precision. The limits of detection for both instruments are presented in Table S2 (ng m^{-3}).

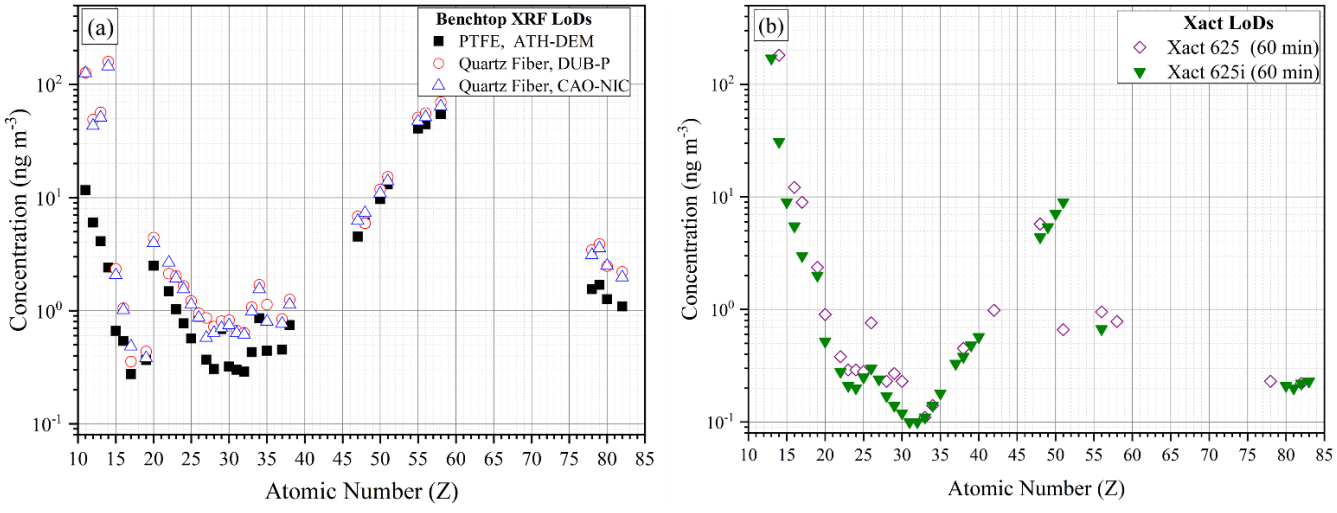

Figure 2: Limits of detections for the benchtop XRF spectrometer, for PTFE and Quartz fiber filters in ng m^{-3}. b) Limits of detections for the Xact 625 and 625i for 60-minute time resolution.

3 Results

3.1 Impact of PTFE and Quartz fiber filter substrates on aerosol elemental analysis with ED-XRF

In this study, benchtop ED-XRF measurements were performed on quartz fiber filters at the CAO-NIC and DUB-P sites. Because the characteristic X-ray signal response can depend on the filter matrix and thickness, it is essential to assess substrate-

https://doi.org/10.5194/egusphere-2025-5977
Preprint. Discussion started: 6 January 2026

related effects prior to comparing data from the two systems. Evaluating the behaviour of PTFE versus quartz fiber filters therefore provides a necessary basis to ensure that observed differences between the benchtop XRF and the Xact originate from instrument performance and aerosol characteristics, rather than from substrate-induced analytical bias.

The comparison of ED-XRF measurements on PTFE and quartz fiber filters underscores the influence of aerosol penetration into the quartz matrix, particularly affecting low-energy X-rays (light elements). PTFE filters, with a typical thickness of 40–50 µm, retain particles on the surface and are thus considered "infinitely thin" for XRF analysis (Chiari et al., 2018). In contrast, quartz filters— with thickness approximately at 400–600 µm —act as bulk substrates, with particles depositing both on the surface and up to ~20 µm deep (Castaneda et al., 1998; Žitnik et al., 2008). Additionally, SEM analysis by Suárez-Peña et al. (2016) confirmed the isotropic structure of quartz fibers, showing non-uniform voids and deep particle penetration, especially for submicron aerosols. Particles <1 µm can reach depths beyond 300 µm, with those 0.1–0.5 µm accumulating in the inner layers (300–600 µm) due to Brownian diffusion, while larger particles are captured in the outer layers via interception and impaction.

When using quartz fiber filters, attenuation effects impact the measurement of light elements by weakening low-energy X-rays. Aerosol particles that penetrate the filter matrix experience filter attenuation, where emitted X-rays are absorbed by the filter material before escaping. Additionally, the strong Si signal from quartz fiber filters not only hinders the precise measurement of lighter elements (Na, Mg, and Al) but also significantly enhances the spectral background which further complicates the detection of these elements, reducing measurement accuracy and sensitivity. In contrast, PTFE filters, which retain particles on the surface, minimize this effect.

To assess the impact of filter type on ED-XRF measurements, we compared elemental concentrations from 21 quartz fiber and 21 Teflon 24-hour PM_{10} filters (Section 2.1), evaluating differences due to particle penetration and X-ray attenuation. Although this comparison was performed on PM_{10} samples, it remains highly relevant to our $PM_{2.5}$ dataset, as the elements most affected by attenuation — S, Cl, K—are primarily associated with fine fraction aerosols. Gini et al. (2022) reported that fine elemental Sulfur, mainly present as sulfate (SO_4^{2-}), originates from anthropogenic sources and is predominantly found in the submicron range (0.1–1 µm). Similarly, potassium exhibits a bimodal distribution, but its fine fraction—linked to biomass burning—remains the dominant one.

Linear regressions through the origin ($y = ax$) were performed to capture the proportional attenuation caused by the quartz filters, without introducing a baseline offset, because both filters were exposed to the same aerosol loading. The comparison between PTFE and Quartz fiber filters yielded strong correlations ($R^2 \geq 0.95$) across all analysed elements. Slopes represent the ratio of Teflon to quartz fiber concentrations, with values above unity indicating attenuation by the quartz filter. S exhibited the highest slope (1.87 ± 0.05), followed by Cl (1.51 ± 0.08) and K (1.48 ± 0.06), suggesting enhanced attenuation (Table 1). In contrast, elements such as Ca (1.00 ± 0.01), Fe (0.95 ± 0.08), showed slopes near unity, consistent with minimal filter-induced effects for heavier elements.

https://doi.org/10.5194/egusphere-2025-5977
Preprint. Discussion started: 6 January 2026

Table 1: Linear regression slopes for each element comparing quartz fiber and Teflon filters.

Element	Slope
S	1.87 ± 0.05
Cl	1.51 ± 0.08
K	1.48 ± 0.06
Ca	1.00 ± 0.01
Ti	0.95 ± 0.02
Fe	0.95 ± 0.01
Ni	1.04 ± 0.04
Cu	0.98 ±0.02
Zn	1.07 ± 0.01

Based on these results, correction factors of 1.87, 1.51, and 1.48 were applied to S, Cl, and K measurements, respectively, while no corrections were applied to Ca, Ti, Fe, Ni, Cu, and Zn due to slopes close to unity and negligible substrate influence.

Additionally, from the recent study of Unga et al. (2025) on PM_{10} filters, it is shown that quartz fiber filters systematically yield lower concentrations for light elements such as S, Cl, and K compared to Teflon substrates (~0.6–0.7 C_{quartz}/C_{Teflon} ratios). Our results agree with this trend, as the Teflon/quartz fiber slopes obtained here for S (1.87), Cl (1.51), and K (1.48) (Table 1) correspond to inverse ratios of approximately 0.5–0.7, confirming similar attenuation effects in quartz fiber substrates for light elements. Figure 3 displays the comparison of elemental concentrations between Teflon and quartz fiber filters for S, K, Ca, and Fe.

https://doi.org/10.5194/egusphere-2025-5977
Preprint. Discussion started: 6 January 2026

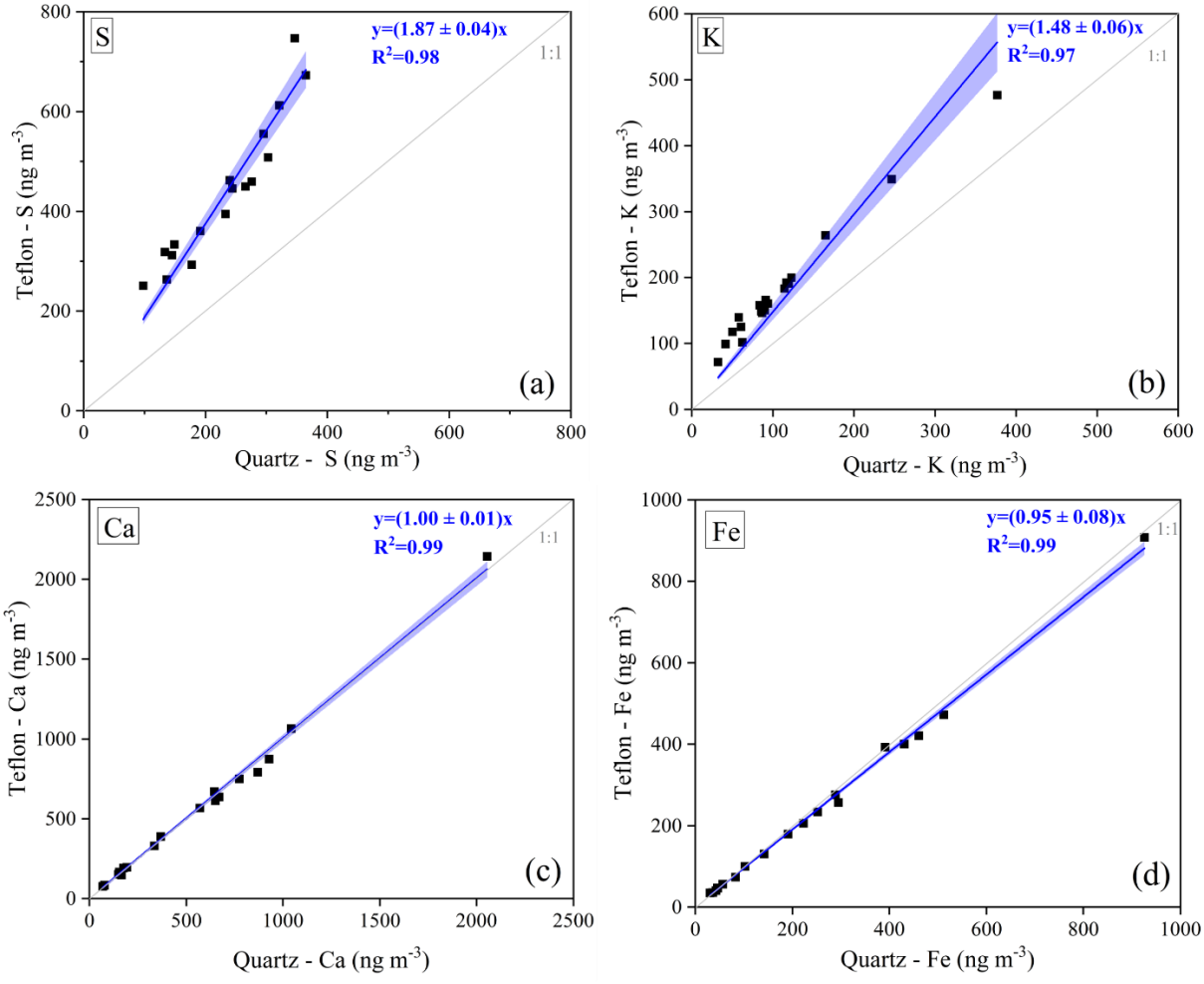

255 **Figure 3: Comparison of Elemental Concentrations: Teflon vs. Quartz Filters of S (a), K (b), Ca (c) and Fe (d).**

To further investigate attenuation effects, we simulated the characteristic intensities of S, Cl and K as a function of quartz fiber thickness utilizing the XMI-MSIM code (Schoonjans et al., 2013). The simulation incorporated the X-ray excitation energy (3.69 keV), spectrometer geometry, and detector characteristics of the Panalytical Epsilon 5 ED-XRF system.
260 For quartz fiber thicknesses ranging from 1 to 450 µm, the normalized X-ray intensity showed a marked decrease due to absorption within the filter matrix. At 100 µm, the transmitted intensity dropped to approximately 0.30 for S, 0.36 for Cl, and 0.46 for K, confirming significant attenuation for lighter elements as the thickness of the quartz fiber filter increases (Figure 4).

https://doi.org/10.5194/egusphere-2025-5977
Preprint. Discussion started: 6 January 2026

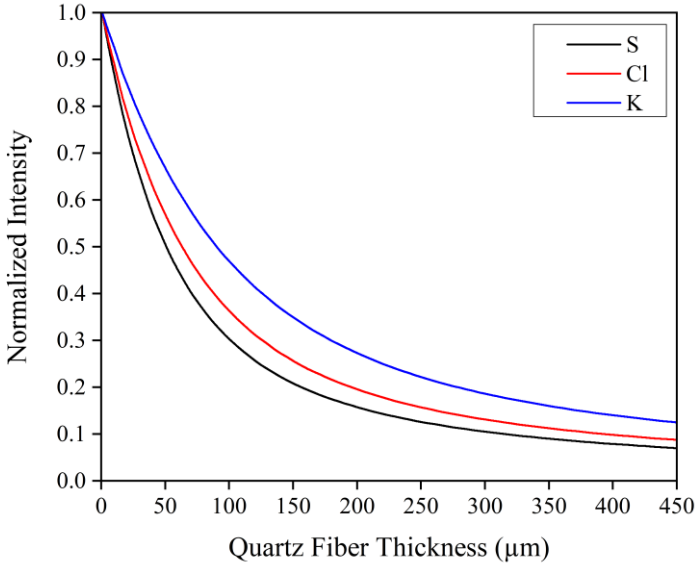

Figure 4: Normalized intensity of S, Cl and K as a function of quartz fiber thickness filter using the XMI-MSIM simulation code.

3.2 Comparative Analysis of NRT-XRF Monitors and Benchtop XRF Spectrometer: Data Processing

For the comparison between the NRT-XRF monitors (Xact 625 and Xact 625i) and the filter samples analysed by the benchtop XRF spectrometer, the hourly Xact measurements from corresponding days were averaged to match the 24-hour filter sample periods. Each 24-hour cycle included 23.5 hourly values from the Xact instruments, while the remaining half hour is utilized for the system's calibration check. For calculating the 24-hour average value, any hourly values reported below the LOD were substituted with LOD/2. Additionally, when quartz fiber filters were used, the measured concentrations of S, Cl, and K were multiplied by correction factors of 1.87, 1.51, and 1.48, respectively (Table 1).

For the quantitative analysis only values above the limit of quantification (LOQ) were used in the comparison, to ensure accuracy and reliability. The LOQ, defined as three times the limit of detection, represents the lowest concentration that can be quantified with acceptable precision and accuracy.

Linear regressions were performed using the model $y=ax+b$, as including an intercept allows detection of systematic offsets between instruments and avoids biasing the slope, consistent with best practice in instrument inter-comparison studies. In addition, 95% confidence intervals from the least-squares fit were included in the regression plots to illustrate the uncertainty in the relationship between the instruments.

3.3 Benchtop XRF (PTFE) vs Xact 625i

Teflon filter samples analysed using the benchtop XRF system were compared with the corresponding Xact 625i measurements for eight elements (Si, S, Cl, K, Ca, Ti, Fe, and Zn). The linear regression slope and coefficient of determination (R^2) for each element are summarized in Table 2. Figure 5 presents the regression curves for Si, S, Fe, and Zn, while Figure 6 shows the

https://doi.org/10.5194/egusphere-2025-5977
Preprint. Discussion started: 6 January 2026

time series graphs for S and Fe. Regression plots and time series for the remaining elements are provided in the Supplementary Information (SI).

Table 2: Summary of linear regression slopes and R^2 values for each element at the ATH-DEM, CAO-NIC, and DUB-P stations.

	ATH-DEM station		CAO-NIC station		DUB-P station	
Element	**Slope**	**R^2**	**Slope**	**R^2**	**Slope**	**R^2**
Si	0.94 ± 0.19	0.88	–	–	–	–
S	0.97 ± 0.01	0.99	1.20 ± 0.07	0.49	1.58 ± 0.06	0.93
Cl	1.18 ± 0.09	0.95	3.10 ± 0.18	0.62	2.63 ± 0.13	0.89
K	0.66 ± 0.03	0.94	0.89 ± 0.02	0.83	0.78 ± 0.13	0.42
Ca	0.54 ± 0.04	0.88	1.72 ± 0.03	0.93	2.03 ± 0.30	0.66
Ti	0.72 ± 0.13	0.84	1.43 ± 0.03	0.94	–	–
V	–	–	–	–	1.37 ± 0.06	0.96
Mn	–	–	1.05 ± 0.06	0.81	–	–
Fe	0.66 ± 0.03	0.94	1.47 ± 0.03	0.91	1.63 ± 0.37	0.29
Ni	–	–	–	–	1.25 ± 0.12	0.78
Cu	–	–	0.67 ± 0.05	0.72	–	–
Zn	0.89 ± 0.10	0.77	1.02 ± 0.03	0.87	1.36 ± 0.13	0.81
Sr	–	–	0.63 ± 0.17	0.51	–	–
Pb	–	–	0.46 ± 0.14	0.15	–	–

Only four measurements for silicon (Si) were above the limit of quantification (LOQ) for the Xact 625i, reflecting the spectrometer's limited sensitivity for this element. This highlights one of the key limitations of the Xact 625i compared to the benchtop XRF system—its generally higher limits of detection (LoDs) in the lighter elements like Si, which can hinder accurate quantification, particularly for elements with low ambient concentrations. Nevertheless, for the Si data points above the LOQ, a slope of 0.94 ± 0.19 (R^2 = 0.88) was observed, indicating strong agreement between the instruments. In contrast, sulfur (S) exhibited excellent performance across both systems, with a slope of 0.97 ± 0.01 and an R^2 of 0.99, demonstrating a near-perfect correlation and underscoring the Xact 625i's robustness in measuring this element. Chlorine (Cl) demonstrated a slope of 1.18 ± 0.09 (R^2 = 0.95), indicating a strong correlation with a slight deviation from unity. Potassium (K) showed a slope of 0.66 ± 0.03 (R^2 = 0.94), suggesting consistent trends despite a systematic difference in concentrations. Calcium (Ca) and titanium (Ti) exhibited slopes of 0.54 ± 0.04 (R^2 = 0.88) and 0.72 ± 0.13 (R^2 = 0.84), respectively. Iron (Fe) displayed a slope of 0.66 ± 0.03 (R^2 = 0.94), indicating strong agreement. Although the slopes below unity suggest systematic underestimation by the Xact 625i for some elements, the consistently high R^2 values confirm reliable and reproducible trends across both systems. Zinc (Zn), with a slope of 0.89 ± 0.10 (R^2 = 0.77), showed moderate correlation, where the slope near unity reflected comparable measurements, while the lower R^2 indicated greater variability.

https://doi.org/10.5194/egusphere-2025-5977
Preprint. Discussion started: 6 January 2026

The average slope of 0.82 and average R^2 of 0.91 indicated a strong overall correlation between the benchtop XRF spectrometer and the Xact 625i, suggesting that both instruments produced consistent measurements across most elements. The slope slightly below 1 implied a systematic difference in quantification, where the Xact 625i tended to report lower values compared to the benchtop XRF.

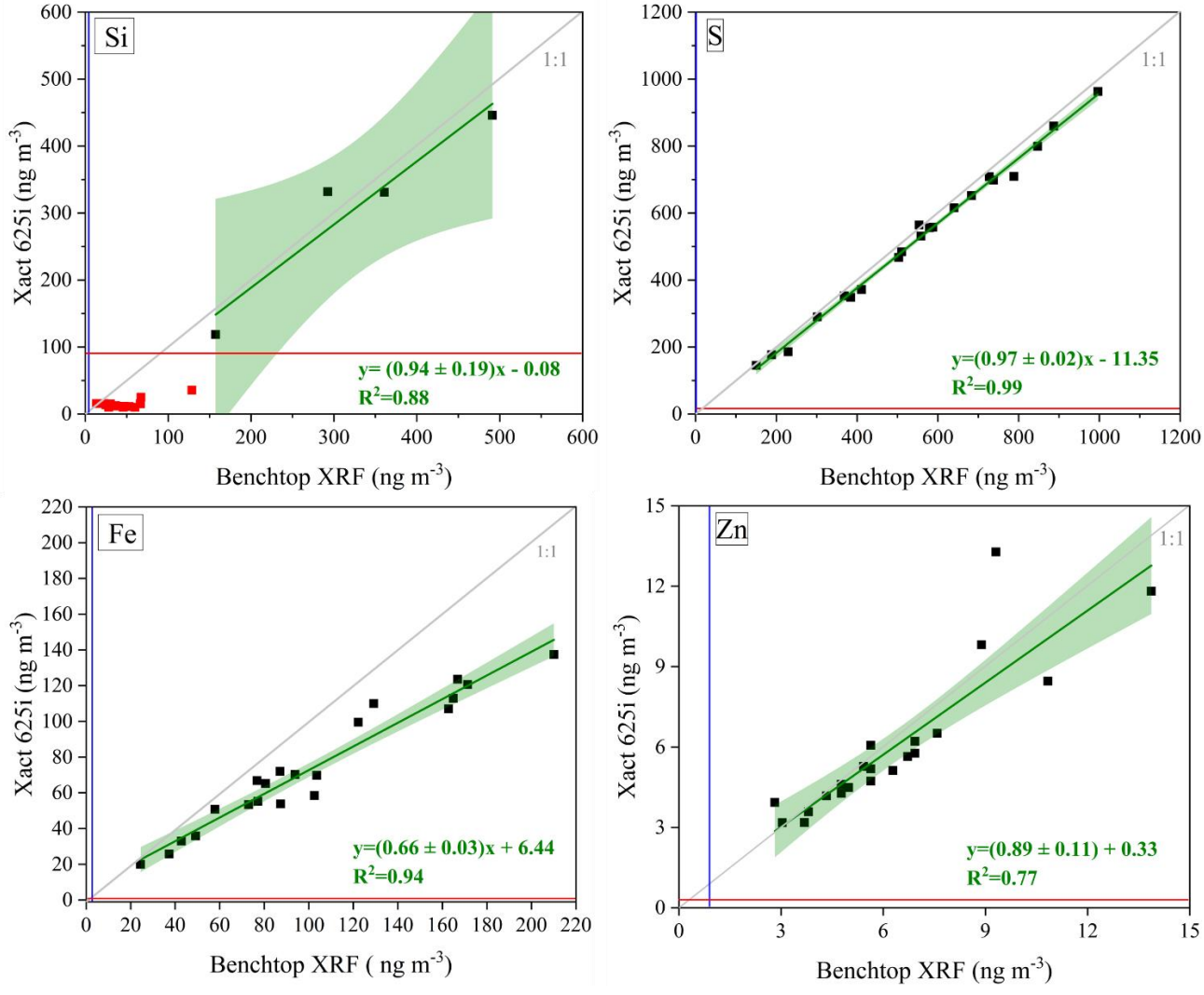

Figure 5: Comparison of elemental concentrations in ng m^{-3} for Si, S, Fe, and Zn for the ATH-DEM station. The blue lines indicate the LOQ threshold for the benchtop XRF spectrometer, while the red lines represent the corresponding threshold for the Xact 625i continuous elemental monitor. The grey line represents the 1:1 reference line, while the green line represents the linear regression fit. Data points below the LOQ were excluded from the analysis to ensure accurate comparison between the two instruments and are highlighted in red, distinguishing measurements with higher uncertainty.

https://doi.org/10.5194/egusphere-2025-5977
Preprint. Discussion started: 6 January 2026

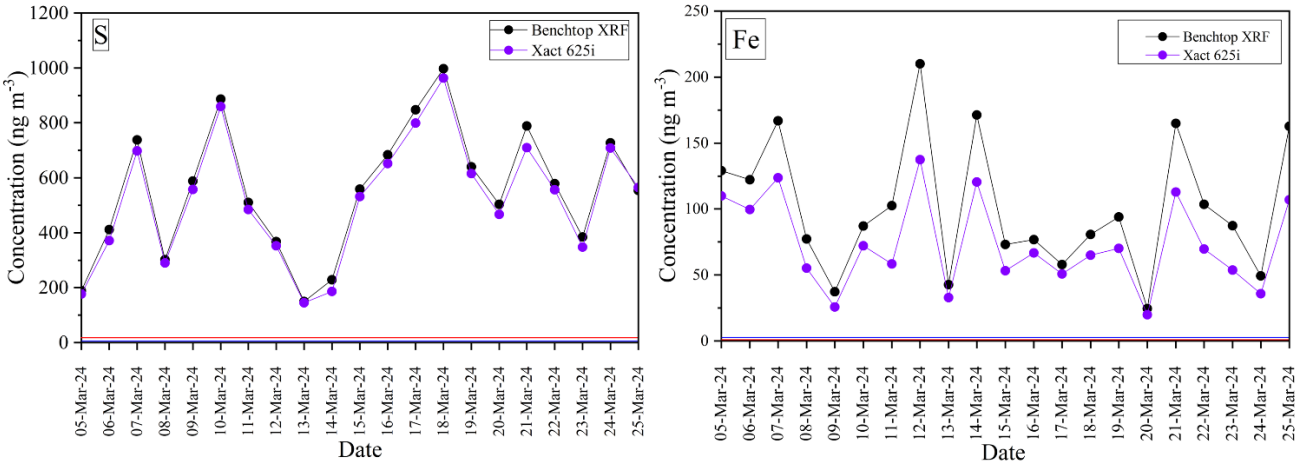

Figure 6: Time series graphs comparing S and Fe concentrations (ng m⁻³) from March 5 to 25, 2024, show strong agreement for S, while Fe exhibits a consistent deviation, with lower values reported by the Xact 625i. This suggests differences in the calibration curves for heavier elements between the instruments. The red and blue lines indicate the LOQ thresholds for the Xact 625i and the benchtop XRF spectrometer, respectively.

3.4 Benchtop XRF (Quartz Fiber) vs Xact 625i

At the CAO-NIC site, benchtop XRF measurements were performed on quartz fiber filters. Table 2 presents the linear regression slopes and R^2 values for each element, compared with the corresponding Xact 625i measurements. Figure 7 presents the regression curves for S, Cl, K and Zn, while Figure 8 shows the time series graphs comparing K and Zn. Regression plots and time series for the remaining elements are provided in Supplementary Information (SI).

Sulfur (S) exhibited a slope of 1.20 ± 0.15 (R^2 = 0.49), reflecting moderate agreement between the instruments and some remaining variability after correction. Chlorine (Cl) presented a slope of 3.10 ± 0.18 (R^2 = 0.62), indicating a moderate relationship with higher variability relative to unity, which may relate to particle penetration and absorption within the quartz matrix as well as potential chloride volatility (e.g., ammonium chloride loss). Potassium (K) showed a slope of 0.89 ± 0.07 (R^2 = 0.83), demonstrating good agreement between systems. While the applied correction factors substantially improved the comparability of light-element measurements, minor residual differences remain. These are likely linked to the heterogeneous structure and variable porosity of quartz fiber filters, which can influence attenuation differently between batches, along with instrument-specific and site-dependent aerosol characteristics. Thus, small deviations are expected, but overall, the applied corrections significantly enhance consistency and reliability across the two platforms.

Calcium (Ca) and titanium (Ti) displayed slopes of 1.72 ± 0.03 (R^2 = 0.93) and 1.43 ± 0.03 (R^2 = 0.94), respectively, both showing high correlation and comparable measurements. Manganese (Mn) had a slope of 1.05 ± 0.06 (R^2 = 0.81), indicating strong agreement. Iron (Fe) exhibited a slope of 1.47 ± 0.03 (R^2 = 0.91), reflecting a consistent trend between instruments. Copper (Cu) had a slope of 0.67 ± 0.05 (R^2 = 0.72), suggesting a moderate correlation with some variability. Zinc (Zn) presented a slope of 1.02 ± 0.03 (R^2 = 0.87), indicating highly comparable measurements. Strontium (Sr) exhibited a

https://doi.org/10.5194/egusphere-2025-5977
Preprint. Discussion started: 6 January 2026

slope of 0.63 ± 0.17 (R^2 = 0.51), indicating moderate agreement with some residual variability, while lead (Pb) remained lower at 0.46 ± 0.14 (R^2 = 0.15), reflecting weaker correlation and higher measurement uncertainty.

In addition to the overall agreement, several distinct events were observed where elemental concentrations peaked simultaneously in both the Xact 625i and the benchtop XRF measurements, particularly for calcium (Ca), titanium (Ti), iron (Fe) and manganese (Mn). During these events, the time series from both instruments showed consistent patterns, indicating that they captured the same atmospheric variability. However, the Xact 625i consistently reported higher concentrations, which is likely attributable to differences in the calibration procedures between the two instruments.

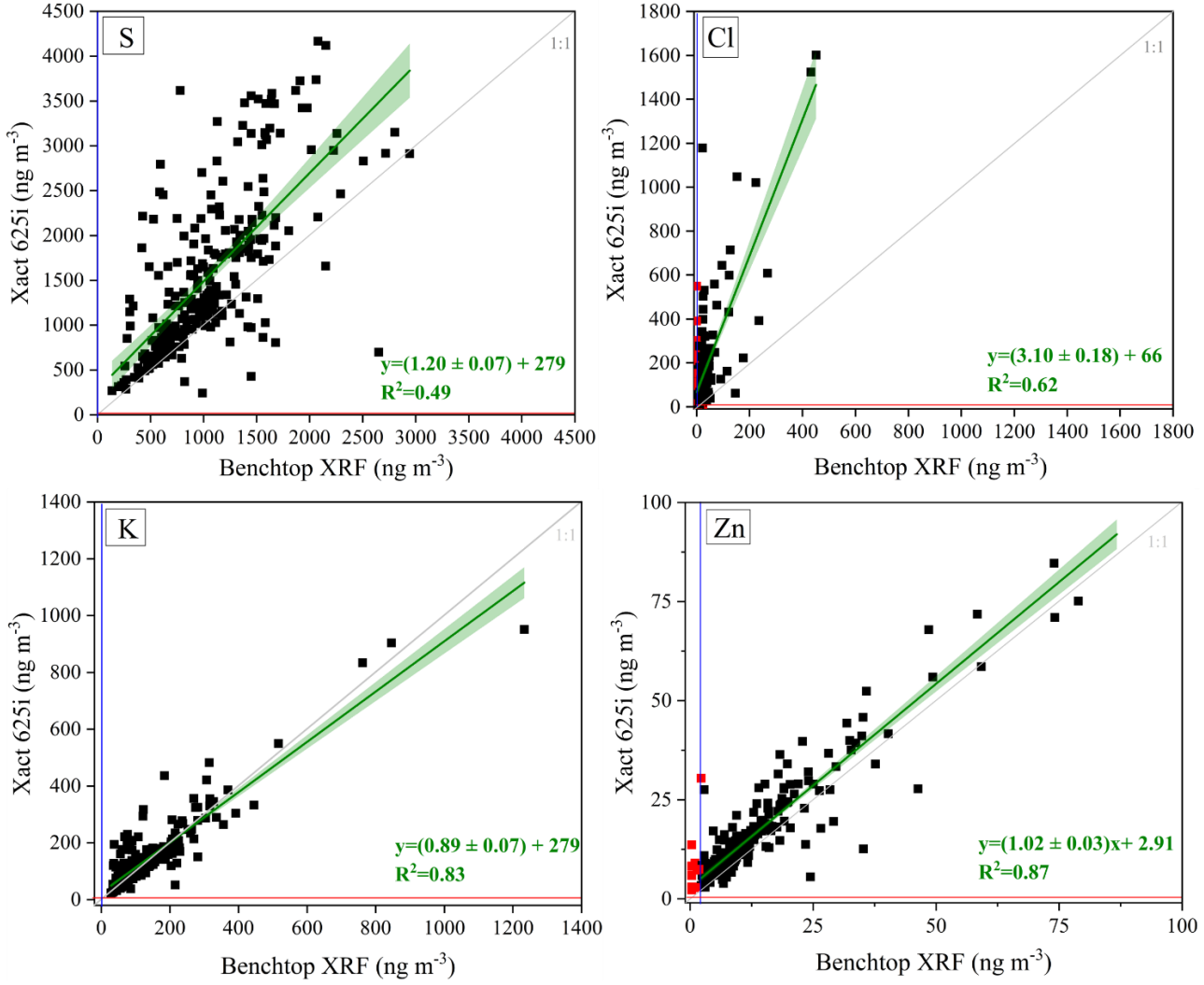

Figure 7: Comparison of elemental concentrations in ng m^{-3} for S, Cl, K and Zn for the CAO-NIC station. The blue lines indicate the LOQ thresholds for the benchtop XRF spectrometer, while the red lines represent the corresponding thresholds for the Xact 625i continuous elemental monitor. The grey line represents the 1:1 reference line, while the green line represents the linear regression fit. Data points below the LOQ were excluded from the analysis to ensure accurate comparison between the two instruments and are highlighted in red, distinguishing measurements with higher uncertainty.

https://doi.org/10.5194/egusphere-2025-5977
Preprint. Discussion started: 6 January 2026

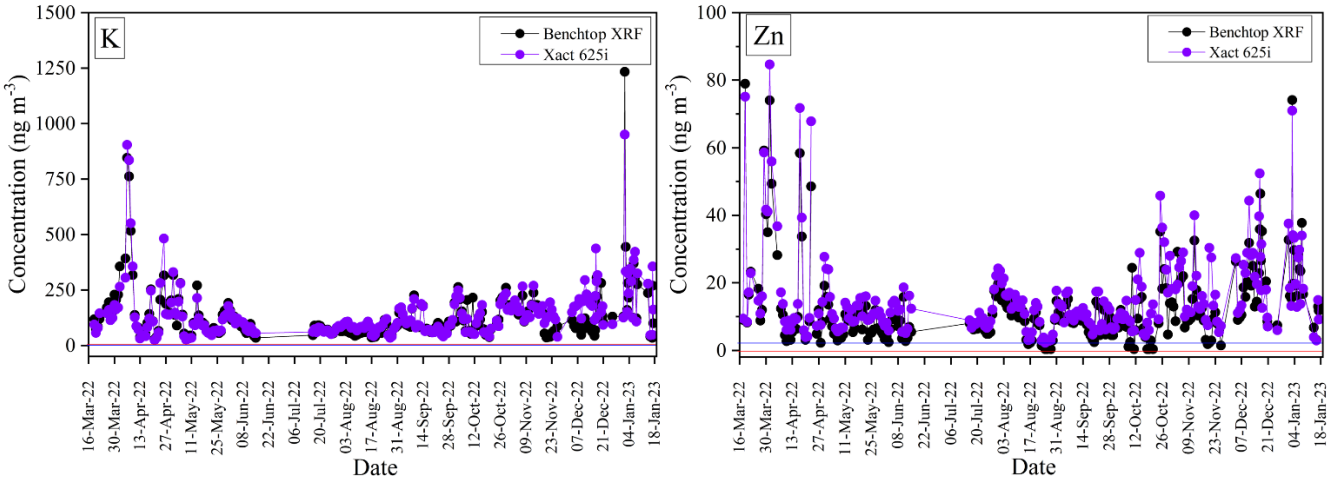

Figure 8: Time series graphs comparing K and Zn concentrations in ng m^{-3} from 16 March 2022 to 18 January 2023. The red and blue lines indicate the LOQ thresholds for the Xact 625i and the benchtop XRF spectrometer, respectively.

3.5 Benchtop XRF (Quartz Fiber) vs Xact 625

Figure 9 presents the regression curves for the elements S, Cl, V, and Ni, while Figure 10 shows the time series graphs for Cl and Zn. Regression plots and time series for the remaining elements are provided in the Supplementary Information (SI). Benchtop XRF measurements were performed on quartz fiber filters collected at the DUB-P site. Sulfur (S) displayed a slope of 1.58 ± 0.06 (R^2 = 0.93), indicating strong agreement between the instruments. Chlorine (Cl) showed the highest slope at 2.63 ± 0.13 (R^2 = 0.89), suggesting a systematic difference while maintaining a strong correlation. Potassium (K) had a slope of 0.78 ± 0.13 (R^2 = 0.42), reflecting a weaker correlation and more variability in the measurements. Calcium (Ca) demonstrated a slope of 2.03 ± 0.30 (R^2 = 0.66), indicating a notable deviation from unity with moderate agreement. Vanadium (V) exhibited a slope of 1.37 ± 0.06 (R^2 = 0.96), reflecting excellent correlation and comparable measurements. Iron (Fe) showed a slope of 1.63 ± 0.37 (R^2 = 0.29), indicating substantial variability and a weaker relationship. Nickel (Ni) had a slope of 1.25 ± 0.12 (R^2 = 0.78), representing reasonable agreement with some deviation. Zinc (Zn) displayed a slope of 1.36 ± 0.13 (R^2 = 0.81), showing a strong correlation between the two instruments. Table 2 presents the linear regression slopes and R^2 values for each element at the DUB-P station.

The average slope of 1.6 and average R^2 of 0.7 for the DUB-P campaign indicated a moderate overall agreement between the benchtop XRF spectrometer and the Xact 625. Although the correlation varies across elements, the results highlight consistent trends for most elements, with stronger agreement for sulfur (S), vanadium (V), and zinc (Zn), while potassium (K) and iron (Fe) exhibited greater variability.

https://doi.org/10.5194/egusphere-2025-5977
Preprint. Discussion started: 6 January 2026

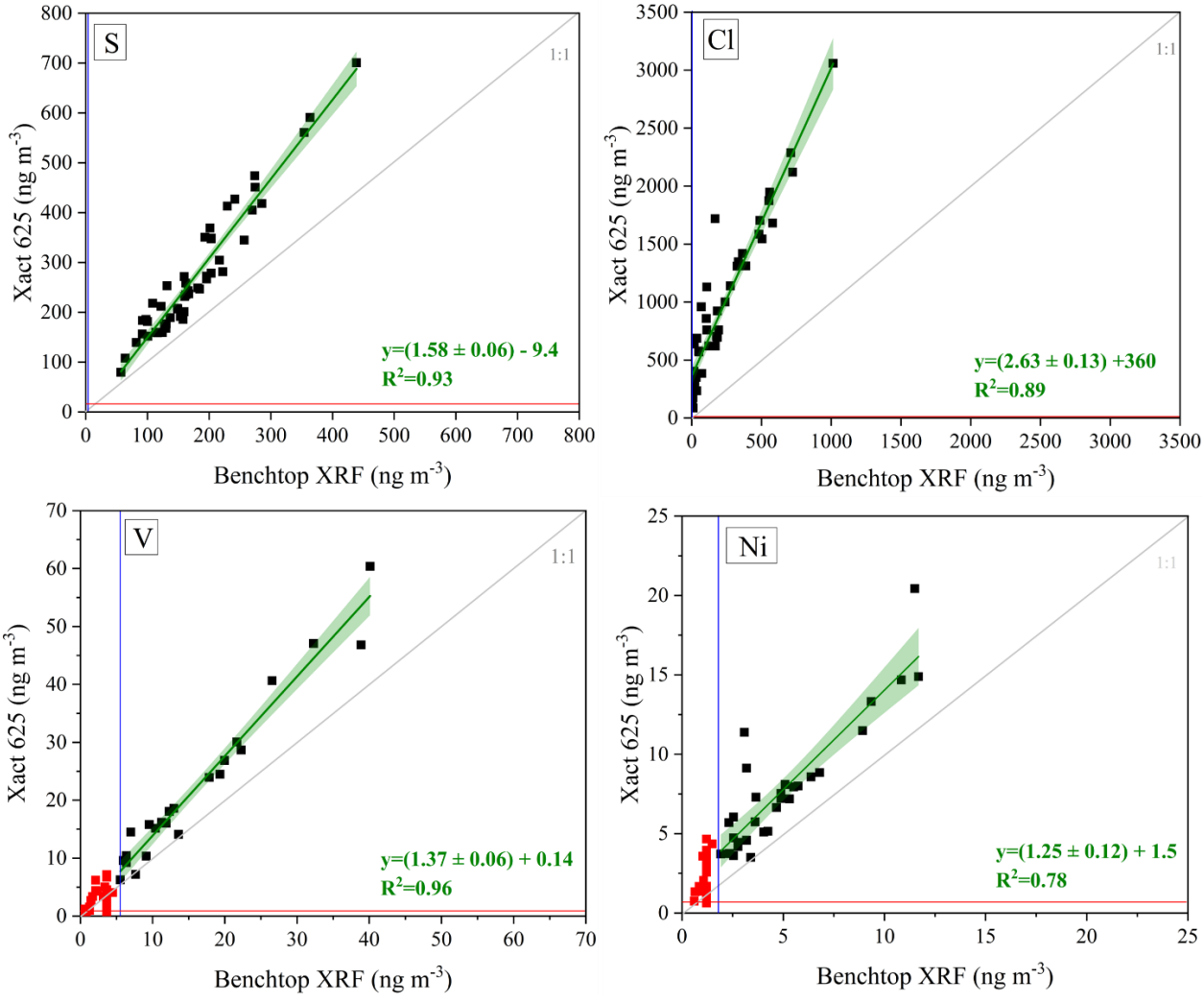

Figure 9: Comparison of elemental concentrations in ng m^{-3} for S, Cl, V and Ni for the DUB-P station. The blue lines indicate the LOQ thresholds for the benchtop XRF spectrometer, while the red lines represent the corresponding thresholds for the Xact 625 continuous elemental monitor. The grey line represents the 1:1 reference line, while the green line represents the linear regression fit. Data points below the LOQ were excluded from the analysis to ensure accurate comparison between the two instruments and are highlighted in red, distinguishing measurements with higher uncertainty.

https://doi.org/10.5194/egusphere-2025-5977
Preprint. Discussion started: 6 January 2026

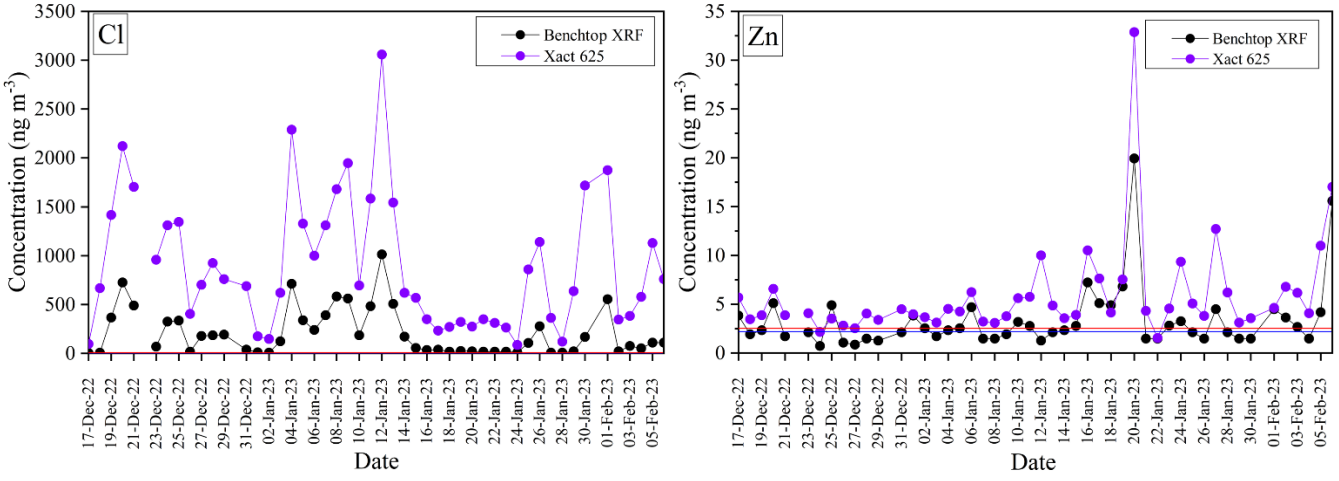

Figure 10: Time series graphs comparing Cl and Zn concentrations (ng m⁻³) at the Dub-P station, show a systematic difference, with the benchtop XRF consistently reporting lower concentrations than the Xact 625. This suggests that the quartz fiber filter may introduce systematic deviations, particularly for light elements, while differences in calibration curves between the instruments could also play a role. The red and blue lines indicate the LOQ thresholds for the Xact 625 and the benchtop XRF spectrometer, respectively.

4 Discussion

The effect of filter type on measurement consistency is evident across the three sites. At ATH-DEM (PTFE filters) the comparison between the Xact 625i and the benchtop XRF spectrometer shows slopes consistently closer to unity for most elements. The consistently high R^2 values (≥ 0.77) across most elements suggest minimal variability, meaning the continuous XRF monitors provides results comparable to those from the benchtop XRF. However, it has to be noted that while the agreement for Si is encouraging, it also highlights the generally higher limits of detection (LoDs) of the Xact 625i for lighter elements (K and below), which can limit its sensitivity in low-concentration environments. Other elements, such as chlorine (Cl), iron (Fe), and potassium (K), also show high R^2 values (≥ 0.77) despite deviations in slope, suggesting systematic differences rather than random variability. These systematic deviations are likely due to differences in instrument calibration, as each system may utilize distinct reference standards. Overall, the better alignment at ATH-DEM is likely aided by the lower X-ray attenuation associated with PTFE filters. Cadeo et al., (2025) recently reported strong agreement between the Xact 625i and benchtop XRF using Teflon filters in Milan, with R^2 values up to 0.99 and slopes generally near unity for most elements, particularly metals. Similarly, our Athens comparison using PTFE filters showed high consistency across eight elements (average slope = 0.82, average R^2 = 0.91), with S and Si near unity and K, Ca, Ti and Fe showing slopes below one but strong correlations ($R^2 > 0.84$). Both studies therefore confirm that the Xact 625i performs robustly on Teflon substrates, providing reliable elemental time-series information with element-specific slope differences.

Despite the application of correction factors, the quartz fiber filter sites (DUB-P and CAO-NIC) continue to exhibit systematic deviations, particularly for lighter elements such as S, Cl, and K. Notably, S shows substantial higher concentrations

https://doi.org/10.5194/egusphere-2025-5977
Preprint. Discussion started: 6 January 2026

at DUB-P, with a corrected slope of 1.58 ± 0.06, compared to a closer-to-unity value of 1.20 ± 0.07 at CAO-NIC. This difference is notable, especially considering the strong correlation at DUB-P ($R^2 = 0.93$), which implies consistent tracking of variability but a persistent offset in absolute values. One possible explanation for this discrepancy lies in the instrumental differences between the two sites: DUB-P employed the Xact 625, while CAO-NIC used the newer Xact 625i. This suggests a potential improvement in calibration or measurement accuracy in the upgraded version. Additionally, iron (Fe) shows poorer agreement at DUB-P, whereas elements like vanadium (V), nickel (Ni), and zinc (Zn) display relatively better performance. This contrast may reflect slight calibration mismatches or performance limitations specific to the older Xact 625 model.

At the CAO-NIC site, the comparison with the Xact 625i reveals both strong correlations and systematic differences across elements. Several elements, including Ca, Ti, Fe, Mn, and zinc (Zn), exhibit high R^2 values (≥ 0.81) and slopes near unity, indicating good agreement between the continuous and benchtop XRF systems. In contrast, chlorine (Cl) shows an elevated slope of 3.10± 0.18 ($R^2 = 0.70$), continuing the pattern seen at DUB-P, where the slope is 2.63 ± 0.13 ($R^2 = 0.89$). Cl is the most noteworthy element, with substantial deviations in slope at both sites, even after the application of correction factors. Despite efforts to account for the attenuation effects, the difference in slope for Cl is far more significant than for other light elements. This suggests that there may be an underlying issue with the Cl measurement itself, which may be attributed to the volatility of the element. Additionally, peak events in elemental concentrations—particularly for Ca, Ti, Fe, and Mn—were observed in both instruments, confirming their ability to track atmospheric variability. However, the Xact 625i systematically reported higher concentrations, further supporting the role of calibration differences. Despite those differences, the overall strong average R^2 of 0.73 and the robust agreement for many mid-to-heavy elements underscore the utility of the Xact 625i, while reinforcing the need for caution when interpreting light elements on quartz filters.

Overall, the filter type significantly influences measurement consistency. PTFE filters, as used at ATH-DEM, result in stronger agreement and more stable measurements across most elements. Quartz fiber filters, used at DUB-P and CAO-NIC, exhibit greater variability for light elements; however, correction efforts mitigate these effects and improve overall comparability, especially for S and K. Figure 11 presents the comparative concentration plots for the elements S, Cl, K, Ca, Ti, Fe and Zn between the continuous and benchtop XRF systems.

https://doi.org/10.5194/egusphere-2025-5977
Preprint. Discussion started: 6 January 2026

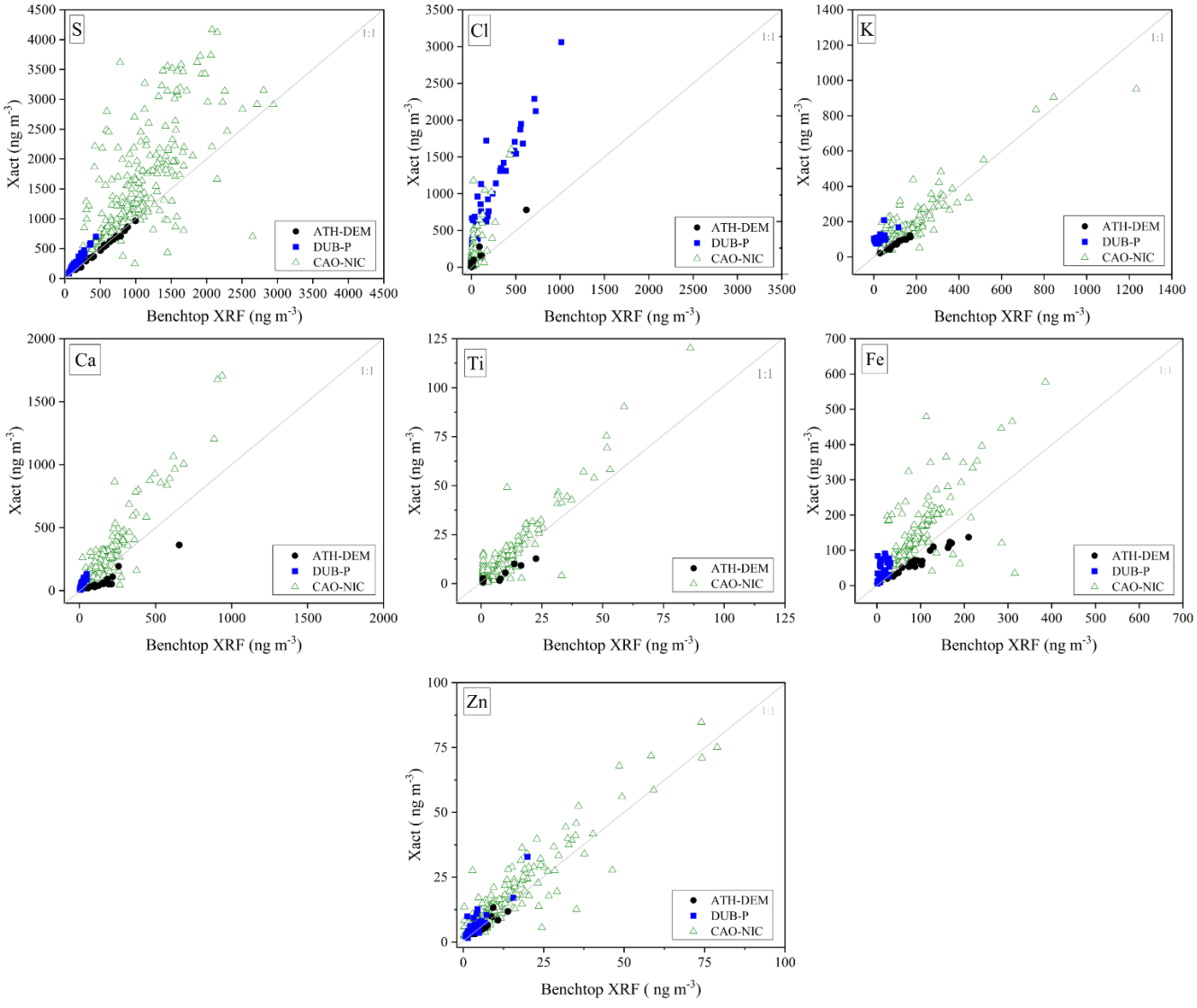

435

Figure 11: Comparison of elemental concentrations of S, Cl, K, Ca, Ti (Ti was not detected in DUB-P), Fe, Zn in ng m^{-3} for all stations.

440

https://doi.org/10.5194/egusphere-2025-5977
Preprint. Discussion started: 6 January 2026

5 Conclusions

This study conducted an extensive intercomparison between a benchtop ED-XRF and NRT-XRF spectrometers (Xact 625 and 625i) to evaluate their performance in measuring elemental concentrations in ambient aerosols across three locations: Athens (Greece), Dublin (Ireland), and Nicosia (Cyprus). A key focus was the influence of filter substrate of measurement results.

The findings highlight that filter type plays a critical role in the quantification of light elements. At the Athens site, where PTFE filters were used, the agreement between instruments was stronger, with slopes closer to unity and high R^2 values, indicating stable and consistent performance. In contrast, at the Dublin and Nicosia sites, which used quartz fiber filters, deviations were observed for sulfur (S), chlorine (Cl), and potassium (K) due to X-ray attenuation in the quartz matrix. Applying correction factors substantially improved agreement for S and K, demonstrating their effectiveness in mitigating substrate-related effects. For Cl, however, a residual positive bias remained likely influenced by both quartz interactions and chloride volatility. In addition, variability in quartz fiber filter composition, porosity, and thickness across filter batches may introduce inconsistent attenuation behaviour, complicating the application of a universal correction factor. Overall, while corrections enhanced comparability, quartz substrates still present challenges for light-element quantification. For heavier elements such as iron (Fe), manganese (Mn), and copper (Cu), the impact of filter type was less pronounced, but variations were still present across sites. Zinc (Zn) maintained good agreement across all locations, whereas lead (Pb) exhibited weaker correlation, suggesting additional influencing factors beyond filter type. Differences in the use of different calibration standards of the two instruments may have contributed to these discrepancies.

Overall, this study underscores the complexity of intercomparisons between different XRF instrument types and filter substrates, particularly for light elements. Quartz fiber filters, in particular, introduce greater variability due to enhanced X-ray attenuation. Therefore, when using quartz fiber filters in ambient aerosol studies, it is essential to implement element-specific correction protocols and consider substrate-related uncertainties during data interpretation. For more reliable and consistent measurements, especially of light elements, PTFE filters are recommended. Additionally, harmonization of calibration procedures across instruments may help reduce discrepancies. These findings highlight the importance of carefully selecting both instrumentation and filter media in XRF-based aerosol analysis to ensure data comparability across monitoring networks.

https://doi.org/10.5194/egusphere-2025-5977
Preprint. Discussion started: 6 January 2026

Data availability. A subset of the data supporting the findings of this study will be openly deposited in the Zenodo repository upon article acceptance, in compliance with HORIZON funding requirements. The associated DOI will be provided in the final version of the manuscript.

Author contributions. SP, MIM, DFA, ED, MP, RB, JW, and KE contributed to the conceptualization of the study. SP, MIM, RB, NOS, KNF and SH performed the investigation and data curation. SP, MIM, and RB conducted the formal analysis. SP, MIM, DFA, and ED were responsible for the writing of the original draft preparation. SP, MIM, ED, MP, and RB provided the methodology. EK, MP, SH and JW handled the project administration. MIM, ED, KE, JS and DFA provided supervision. RB, MP, JW, and ED performed the validation. SP was responsible for visualization. All authors contributed to reviewing and editing the manuscript.

Competing interests. The authors declare that they have no conflict of interest.

Financial support. The PortAIR project was funded by the Irish Environmental Protection Agency (EPA) under grant number 2020-CCRP-LS.6, supported by EPA Ireland and the Department of Environment, Climate and Communications. This study has been supported financially by the RIF-EXCELLENCE/0524/0393 and H2020-EMME-CARE (GA 856612) research grant. The work has also been partially supported by European Union's Horizon Europe programme under grant agreement No 101138449 — MI-TRAP.

References

Aikawa, M., & Hiraki, T. (2010). Difference in the use of a quartz filter and a PTFE filter as first-stage filter in the four-stage filter-pack method. Water, Air, and Soil Pollution, 213(1–4), 331–339. https://doi.org/10.1007/S11270-010-0388-Y/FIGURES/7

Aldekheel, M., Farahani, V. J., & Sioutas, C. (2023). Assessing Lifetime Cancer Risk Associated with Population Exposure to PM-Bound PAHs and Carcinogenic Metals in Three Mid-Latitude Metropolitan Cities. Toxics, 11(8), 697. https://doi.org/10.3390/TOXICS11080697/S1

Amato, F., Alastuey, A., Karanasiou, A., Lucarelli, F., Nava, S., Calzolai, G., Severi, M., Becagli, S., Gianelle, V. L., Colombi, C., Alves, C., Custódio, D., Nunes, T., Cerqueira, M., Pio, C., Eleftheriadis, K., Diapouli, E., Reche, C., Minguillón, M. C., Manousakas, M.-I., Maggos, T., Vratolis, S., Harrison, R. M., & Querol, X. (2016). AIRUSE-LIFE+: A harmonized PM speciation and source apportionment in five southern European cities. Atmospheric Chemistry and Physics, 16(5), 3289–3309. https://doi.org/10.5194/acp-16-3289-2016

https://doi.org/10.5194/egusphere-2025-5977
Preprint. Discussion started: 6 January 2026

Bhowmik, H. S., Shukla, A., Lalchandani, V., Dave, J., Rastogi, N., Kumar, M., Singh, V., & Tripathi, S. N. (2022). Inter-comparison of online and offline methods for measuring ambient heavy and trace elements and water-soluble inorganic ions (NO3-, SO42-, NH4+, and Cl-) in PM2.5over a heavily polluted megacity, Delhi. Atmospheric Measurement Techniques, 15(9), 2667–2684. https://doi.org/10.5194/amt-15-2667-2022

Bimenyimana, E., Pikridas, M., Oikonomou, K., Iakovides, M., Christodoulou, A., Sciare, J., & Mihalopoulos, N. (2023). Fine aerosol sources at an urban background site in the Eastern Mediterranean (Nicosia; Cyprus): Insights from offline versus online source apportionment comparison for carbonaceous aerosols. Science of The Total Environment, 893, 164741. https://doi.org/10.1016/J.SCITOTENV.2023.164741

Bimenyimana, E., Sciare, J., Pikridas, M., Oikonomou, K., Iakovides, M., Vasiliadou, E., Savvides, C., & Mihalopoulos, N. (2025). Persistent high PM pollution in the Eastern Mediterranean and Middle East: Insights from long-term observations and source apportionment in Cyprus. *EGUsphere*, 1–23. https://doi.org/10.5194/EGUSPHERE-2025-3234

Cadeo, L., Biffi, B., Chazeau, B., Colombi, C., Cosenza, R., Manousakas, M.-I., Daellenbach, K. R., & H Prévôt, A. S. (2025). Intercomparison of online and offline XRF spectrometers for determining the PM10 elemental composition of ambient aerosol. https://doi.org/10.5194/egusphere-2025-110

Caggiano, R., Sabia, S., & Speranza, A. (2019). Trace elements and human health risks assessment of finer aerosol atmospheric particles (PM1). Environmental Science and Pollution Research, 26(36), 36423–36433. https://doi.org/10.1007/S11356-019-06756-W/TABLES/5

Castaneda, C. M., Cahill, T. A., Romero, J. L., & King, R. S. (1998). Depth profiling of hydrogen in amorphous media and applicable to quartz air filters. Nuclear Instruments and Methods in Physics Research Section B: Beam Interactions with Materials and Atoms, 145(4), 553–561. https://doi.org/10.1016/S0168-583X(98)00506-0

Chen, S.-L., Chang, S.-W., Chen, Y.-J., & Chen, H.-L. (2021). Possible warming effect of fine particulate matter in the atmosphere. Communications Earth & Environment 2021 2:1, 2(1), 1–9. https://doi.org/10.1038/s43247-021-00278-5

Chiari, M., Yubero, E., Calzolai, G., Lucarelli, F., Crespo, J., Galindo, N., Nicolás, J. F., Giannoni, M., & Nava, S. (2018). Comparison of PIXE and XRF analysis of airborne particulate matter samples collected on Teflon and quartz fibre filters. Nuclear Instruments and Methods in Physics Research Section B: Beam Interactions with Materials and Atoms, 417, 128–132. https://doi.org/10.1016/J.NIMB.2017.07.031

Christodoulou, A., Stavroulas, I., Vrekoussis, M., Desservettaz, M., Pikridas, M., Bimenyimana, E., Kushta, J., Ivančič, M., Rigler, M., Goloub, P., Oikonomou, K., Sarda-Estève, R., Savvides, C., Afif, C., Mihalopoulos, N., Sauvage, S., & Sciare, J. (2023). Ambient carbonaceous aerosol levels in Cyprus and the role of pollution transport from the Middle East. Atmospheric Chemistry and Physics, 23(11), 6431–6456. https://doi.org/10.5194/ACP-23-6431-2023

Diapouli, E., Manousakas, M. I., Vratolis, S., Vasilatou, V., Pateraki, S., Bairachtari, K. A., Querol, X., Amato, F., Alastuey, A., Karanasiou, A. A., Lucarelli, F., Nava, S., Calzolai, G., Gianelle, V. L., Colombi, C., Alves, C., Custódio, D., Pio, C., Spyrou, C., Kallos, G. B., & Eleftheriadis, K. (2017). AIRUSE-LIFE+: Estimation of natural source contributions to urban

https://doi.org/10.5194/egusphere-2025-5977
Preprint. Discussion started: 6 January 2026

ambient air PM_{10} and $PM_{2.5}$ concentrations in southern Europe – Implications to compliance with limit values. Atmospheric Chemistry and Physics, 17(5), 3673–3685. https://doi.org/10.5194/acp-17-3673-2017

Fossum, K. N., Lin, C., O'Sullivan, N., Lei, L., Hellebust, S., Ceburnis, D., Afzal, A., Tremper, A., Green, D., Jain, S., Byčenkienė, S., O'Dowd, C., Wenger, J., & Ovadnevaite, J. (2024). Two distinct ship emission profiles for organic-sulfate source apportionment of PM in sulfur emission control areas. Atmospheric Chemistry and Physics, 24(18), 10815–10831. https://doi.org/10.5194/ACP-24-10815-2024

Fossum, K., O'Sullivan, N., Jain, S., Lei, L., Lin, C., Ceburnis, D., Hellebust, S., O'Dowd, C., Ovadnevaite, J., & Wenger, J. (2025). Source Apportionment of Air Pollution in the Dublin Port Area (PortAIR). Research 495. Environmental Protection Agency. ISBN 978-1-80009-314-0. https://www.epa.ie/publications/research/air/research-495-source-apportionment-of-air-pollution-in-the-dublin-port-area-portair.php

Furger, M., Minguillón, M. C., Yadav, V., Slowik, J. G., Hüglin, C., Fröhlich, R., Petterson, K., Baltensperger, U., & Prévôt, A. S. H. (2017). Elemental composition of ambient aerosols measured with high temporal resolution using an online XRF spectrometer. Atmospheric Measurement Techniques, 10(6), 2061–2076. https://doi.org/10.5194/amt-10-2061-2017

Furger, M., Rai, P., Slowik, J. G., Cao, J., Visser, S., Baltensperger, U., & Prévôt, A. S. H. (2020). Automated alternating sampling of PM10 and PM2.5 with an online XRF spectrometer. Atmospheric Environment: X, 5, 100065. https://doi.org/10.1016/J.AEAOA.2020.100065

Eleftheriadis, K., Gini, M. I., Diapouli, E., Vratolis, S., Vasilatou, V., Fetfatzis, P., & Manousakas, M. I. (2021). Aerosol microphysics and chemistry reveal the COVID19 lockdown impact on urban air quality. *Scientific Reports 2021 11:1*, *11*(1), 14477-. https://doi.org/10.1038/s41598-021-93650-6

Gini, M., Manousakas, M., Karydas, A. G., & Eleftheriadis, K. (2022). Mass size distributions, composition and dose estimates of particulate matter in Saharan dust outbreaks. Environmental Pollution, 298, 118768. https://doi.org/10.1016/J.ENVPOL.2021.118768

Hopke, P. K., Dai, Q., Li, L., & Feng, Y. (2020). Global review of recent source apportionments for airborne particulate matter. Science of The Total Environment, 740, 140091. https://doi.org/10.1016/J.SCITOTENV.2020.140091

Healy, R. M., O'Connor, I. P., Hellebust, S., Allanic, A., Sodeau, J. R., & Wenger, J. C. (2009). Characterisation of single particles from in-port ship emissions. Atmospheric Environment, 43(40), 6408–6414. https://doi.org/10.1016/J.ATMOSENV.2009.07.039

Huang, R. J., Cheng, R., Jing, M., Yang, L., Li, Y., Chen, Q., Chen, Y., Yan, J., Lin, C., Wu, Y., Zhang, R., El Haddad, I., Prevot, A. S. H., O'Dowd, C. D., & Cao, J. (2018). Source-Specific Health Risk Analysis on Particulate Trace Elements: Coal Combustion and Traffic Emission As Major Contributors in Wintertime Beijing. Environmental Science and Technology, 52(19), 10967–10974. https://pubs.acs.org/doi/10.1021/acs.est.8b02091

https://doi.org/10.5194/egusphere-2025-5977
Preprint. Discussion started: 6 January 2026

Jain, S., Sharma, S. K., Vijayan, N., & Mandal, T. K. (2020). Seasonal characteristics of aerosols (PM2.5 and PM10) and their source apportionment using PMF: A four year study over Delhi, India. Environmental Pollution, 262, 114337. https://doi.org/10.1016/j.envpol.2020.114337

Jang, H. N., Seo, Y. C., Lee, J. H., Hwang, K. W., Yoo, J. I., Sok, C. H., & Kim, S. H. (2007). Formation of fine particles enriched by V and Ni from heavy oil combustion: Anthropogenic sources and drop-tube furnace experiments. Atmospheric Environment, 41(5), 1053–1063. https://doi.org/10.1016/J.ATMOSENV.2006.09.011

Khuzestani, R. B., Schauer, J. J., Wei, Y., Zhang, Y., & Zhang, Y. (2017). A non-destructive optical color space sensing system to quantify elemental and organic carbon in atmospheric particulate matter on Teflon and quartz filters. Atmospheric Environment, 149, 84–94. https://doi.org/10.1016/J.ATMOSENV.2016.11.002

Manousakas, M., Diapouli, E., Papaefthymiou, H., Kantarelou, V., Zarkadas, C., Kalogridis, A.-C., Karydas, A.-G., & Eleftheriadis, K. (2018). XRF characterization and source apportionment of PM10 samples collected in a coastal city. X-Ray Spectrometry, 47(3), 190–200. https://doi.org/10.1002/xrs.2817

Manousakas, M., Diapouli, E., Belis, C., Vasilatou, V., Gini, M., Lucarelli, F., Querol, X., & Eleftheriadis, K. (2021). Quantitative assessment of the variability in chemical profiles from source apportionment analysis of PM10 and PM2.5 at different sites within a large metropolitan area. Environmental Research, 192, 110257. https://doi.org/10.1016/J.ENVRES.2020.110257

Manousakas, M., Furger, M., Daellenbach, K. R., Canonaco, F., Chen, G., Tobler, A., Rai, P., Qi, L., Tremper, A. H., Green, D., Hueglin, C., Slowik, J. G., El Haddad, I., & Prevot, A. S. H. (2022). Source identification of the elemental fraction of particulate matter using size segregated, highly time-resolved data and an optimized source apportionment approach. Atmospheric Environment: X, 14, 100165. https://doi.org/10.1016/J.AEAOA.2022.100165

Megido, L., Suárez-Peña, B., Negral, L., Castrillón, L., & Fernández-Nava, Y. (2017). Suburban air quality: Human health hazard assessment of potentially toxic elements in PM10. Chemosphere, 177, 284–291. https://doi.org/10.1016/J.CHEMOSPHERE.2017.03.009

Ostro, B., Tobias, A., Karanasiou, A., Samoli, E., Querol, X., Rodopoulou, S., Basagaña, X., Eleftheriadis, K., Diapouli, E., Vratolis, S., Jacquemin, B., Katsouyanni, K., Sunyer, J., Forastiere, F., Stafoggia, M., Alessandrini, E., Angelini, P., Berti, G., Bisanti, L., … Pascal, M. (2015). The risks of acute exposure to black carbon in Southern Europe: results from the MED-PARTICLES project. Occupational and Environmental Medicine, 72(2), 123–129. https://doi.org/10.1136/OEMED-2014-102184

Papagiannis, S., Sabur, ·, Abdullaev, F., Vasilatou, V., Manousos, ·, Manousakas, I., Eleftheriadis, K., & Diapouli, E. (2024). Air quality challenges in Central Asian urban areas: a PM2.5 source apportionment analysis in Dushanbe, Tajikistan. Environmental Science and Pollution Research 2024, 1–14. https://doi.org/10.1007/S11356-024-33833-6

https://doi.org/10.5194/egusphere-2025-5977
Preprint. Discussion started: 6 January 2026

Park, S. S., Cho, S. Y., Jo, M. R., Gong, B. J., Park, J. S., & Lee, S. J. (2014). Field evaluation of a near-real time elemental monitor and identification of element sources observed at an air monitoring supersite in Korea. Atmospheric Pollution Research, 5(1), 119–128. https://doi.org/10.5094/APR.2014.015

Rai, P. (2020). Analysis of major and trace elements in ambient aerosols and their sources in European and Asian cities (Doctoral dissertation, ETH Zurich). ETH Zurich Research Collection. https://doi.org/10.3929/ethz-b-000440336

Rai, P., Furger, M., Slowik, J. G., Canonaco, F., Fröhlich, R., Hüglin, C., Minguillón, M. C., Petterson, K., Baltensperger, U., & Prévôt, A. S. H. (2020). Source apportionment of highly time-resolved elements during a firework episode from a rural freeway site in Switzerland. Atmospheric Chemistry and Physics, 20(3), 1657–1674. https://doi.org/10.5194/ACP-20-1657-2020

Rhodes, E. P., Ren, Z., & Mays, D. C. (2012). Zinc leaching from tire crumb rubber. Environmental Science and Technology, 46(23), 12856–12863. https://doi.org/10.1021/ES3024379/SUPPL_FILE/ES3024379_SI_001.PDF

Sailbri Cooper, Inc. - INNOVATION IN MONITORING. (n.d.). Retrieved November 15, 2024, from https://sci-monitoring.com/

Samoli, E., Stafoggia, M., Rodopoulou, S., Ostro, B., Declercq, C., Alessandrini, E., Díaz, J., Karanasiou, A., Kelessis, A. G., Tertre, A. Le, Pandolfi, P., Randi, G., Scarinzi, C., Zauli-Sajani, S., Katsouyanni, K., Forastiere, F., Alessandrini, E., Angelini, P., Berti, G., … Pascal, M. (2013). Associations between fine and coarse particles and mortality in Mediterranean cities: Results from the MED-PARTICLES project. Environmental Health Perspectives, 121(8), 932–938. https://doi.org/10.1289/EHP.1206124

Schoonjans, T., Solé, V. A., Vincze, L., Sanchez Del Rio, M., Appel, K., & Ferrero, C. (2013). A general Monte Carlo simulation of energy-dispersive X-ray fluorescence spectrometers — Part 6. Quantification through iterative simulations. Spectrochimica Acta Part B: Atomic Spectroscopy, 82, 36–41. https://doi.org/10.1016/J.SAB.2012.12.011

Skalny, A. V., Lima, T. R. R., Ke, T., Zhou, J. C., Bornhorst, J., Alekseenko, S. I., Aaseth, J., Anesti, O., Sarigiannis, D. A., Tsatsakis, A., Aschner, M., & Tinkov, A. A. (2020). Toxic metal exposure as a possible risk factor for COVID-19 and other respiratory infectious diseases. Food and Chemical Toxicology, 146, 111809. https://doi.org/10.1016/J.FCT.2020.111809

Suárez-Peña, B., Negral, L., Castrillón, L., Megido, L., Marañón, E., & Fernández-Nava, Y. (2016). Imaging Techniques and Scanning Electron Microscopy as Tools for Characterizing a Si-Based Material Used in Air Monitoring Applications. Materials 2016, Vol. 9, Page 109, 9(2), 109. https://doi.org/10.3390/MA9020109

Thorpe, A., & Harrison, R. M. (2008). Sources and properties of non-exhaust particulate matter from road traffic: A review. Science of The Total Environment, 400(1–3), 270–282. https://doi.org/10.1016/J.SCITOTENV.2008.06.007

Tremper, A. H., Font, A., Priestman, M., Hamad, S. H., Chung, T.-C., Pribadi, A., Brown, R. J. C., Goddard, S. L., Grassineau, N., Petterson, K., Kelly, F. J., & Green, D. C. (2018). Field and laboratory evaluation of a high time resolution x-ray fluorescence instrument for determining the elemental composition of ambient aerosols. Atmos. Meas. Tech, 11, 3541–3557. https://doi.org/10.5194/amt-11-3541-2018

https://doi.org/10.5194/egusphere-2025-5977
Preprint. Discussion started: 6 January 2026

Unga, F., Calzolai, G., Chiari, M., Cuccia, E., Colombi, C., Franciosa, M., Dinoi, A., Merico, E., Pennetta, A., Gómez-Sánchez, N., Mapelli, C., Pareti, S., Perrino, C., Yubero, E., & Contini, D. (2025). Determination of aerosol composition by ED-XRF on Teflon and quartz substrates: potentialities and limits. Aerosol Res, 3, 405–415. https://doi.org/10.5194/ar-3-405-2025

Vecchi, R., Valli, G., Fermo, P., D'Alessandro, A., Piazzalunga, A., & Bernardoni, V. (2009). Organic and inorganic sampling artefacts assessment. Atmospheric Environment, 43(10), 1713–1720. https://doi.org/10.1016/J.ATMOSENV.2008.12.016

Viana, M., Kuhlbusch, T. A. J., Querol, X., Alastuey, A., Harrison, R. M., Hopke, P. K., Winiwarter, W., Vallius, M., Szidat, S., Prévôt, A. S. H., Hueglin, C., Bloemen, H., Wåhlin, P., Vecchi, R., Miranda, A. I., Kasper-Giebl, A., Maenhaut, W., & Hitzenberger, R. (2008). Source apportionment of particulate matter in Europe: A review of methods and results. Journal of Aerosol Science, 39(10), 827–849. https://doi.org/10.1016/J.JAEROSCI.2008.05.007

Windell, L. C., Mbengue, S., Pokorná, P., Schwarz, J., Manousakas, M. I., Papagiannis, S., Ondráček, J., & Ždímal, V. (2025). Xact625i vs PX-375: A Comparative Study of Online XRF Ambient Multi-Metal Monitors. https://doi.org/10.5194/egusphere-2025-2350

Yatkin, S., Gerboles, M., & Borowiak, A. (2012). Evaluation of standardless EDXRF analysis for the determination of elements on PM10 loaded filters. Atmospheric Environment, 54, 568–582. https://doi.org/10.1016/J.ATMOSENV.2012.02.062

Žitnik, M., Pelicon, P., Grlj, N., Karydas, A. G., Sokaras, D., Schütz, R., & Kanngießer, B. (2008). Three-dimensional imaging of aerosol particles with scanning proton microprobe in a confocal arrangement. Applied Physics Letters, 93(9), 94104. https://doi.org/10.1063/1.2976163/764942

Zografou, O., Gini, M., Manousakas, M. I., Chen, G., Kalogridis, A. C., Diapouli, E., Pappa, A., & Eleftheriadis, K. (2022). Combined organic and inorganic source apportionment on yearlong ToF-ACSM dataset at a suburban station in Athens. *Atmospheric Measurement Techniques*, *15*(16), 4675–4692. https://doi.org/10.5194/AMT-15-4675-2022